Clays and Clay Minerals, Vol. 47, No. 6, 683–687, 1999.

DIRECT IMAGING OF ZIRCONIA PILLARS IN MONTMORILLONITE BY ANALYTICAL ELECTRON MICROSCOPY

P.A. CROZIER,[1] M. PAN,[1,†] C. BATEMAN,[2,‡] J.J. ALCARAZ,[2] AND J.S. HOLMGREN[2]

[1] Center for Solid State Science, Arizona State University, Tempe, Arizona 85287-1704, USA
[2] UOP, 50 East Algonquin Rd, Des Plaines, Illinois 60017-5016, USA

Abstract—Analytical electron microscopy was used to confirm the location of pillars of zirconia in pillared montmorillonite. Data show that the pillared clay is of "high" quality, with surface areas ranging from 200 to 250 m^2/g and (001) spacings in the 17–18 Å range. The zirconia-rich pillars were observed using bright-field imaging, annular dark-field imaging, and energy-filtered imaging. The composition of the pillars was confirmed by performing nano-analysis using energy-dispersive X-ray spectroscopy and electron energy-loss spectroscopy. The pillars apparently have an irregular shape <50 Å in size. The shape and relatively large size of the pillars suggest that zirconia dispersion is not ideally distributed in this sample. This study is apparently the first report of electron microscopy observation of pillaring material in clays.

Key Words—Clays, Electron Energy-Loss Spectroscopy, Elemental Mapping, Energy-Filtered Imaging, Image Analysis, Materials Characterization.

INTRODUCTION

The ability to vary the basal spacing in different clays is important in catalysis and other technological applications (Vaughan *et al.*, 1979, 1980; Mitchell, 1990 and articles therein; Bartley, 1988). Pillared clays are microporous materials that may provide alternatives to zeolite catalysts. Current effort includes understanding the mechanisms for pillaring these materials, creating better control of the formation of the basal spacing, and understanding the active sites for the application of interest. X-ray diffraction (XRD) gives the interlamellar spacing and the average crystallite size, but little information about the morphology or the pillaring process. Transmission electron microscopy (TEM) is useful to image small features at, or close to, atomic resolution and to provide important data about defects in the structure. Techniques available in analytical electron microscopy (AEM) can yield information about the morphological and elemental variations on the nanometer scale (Datye and Smith, 1992; Crozier and Pan, 1995).

We were able to use AEM to directly image the pillars in zirconia-pillared montmorillonite. By using a combination of TEM techniques, morphological data were correlated with composition to identify the location of the zirconia (ZrO_2) pillars. After initial detailed characterization of the pillar morphology, simple bright-field imaging techniques could be used to identify the pillars in clays treated in various ways. A zirconia-pillared clay was chosen over an alumina-pillared material, because the higher atomic number of the zirconia pillars relative to the Si, Al, and Mg in the clay provides better contrast.

MATERIALS AND METHODS

Reagents were purchased from Aldrich Chemical Company and used as received. Natural montmorillonite clay, trade name HPM-20, was obtained from American Colloid Company and used as received. Montmorillonite is easily swellable and can be readily pillared using standard techniques. Zirconia-pillared montmorillonite was prepared following Bartley (1988). The zirconia pillars were prepared using hydroxyzirconium cations produced by the solvation of zirconyl chloride. A 0.1 M solution of $ZrOCl_2$ was prepared by diluting a 1.63 M stock solution. After aging for 2 h, 150 mL of the 0.1 M solution was combined with 1000 g of water. This solution was heated to 60°C while being stirred for 16–24 h. HPM-20 montmorillonite (15 g) was added with vigorous stirring. The suspension was heated and stirred for an additional 24 h. The clay was recovered using centrifugation, washed with deionized water until Cl free, dried at 110°C overnight, and then calcined at 550°C in flowing air. XRD was used to determine the $d(001)$-value of the "as prepared" and calcined clays; in both cases the (001) spacing was 17–18 Å. The surface areas of the clays were determined by BET analysis (Brunauer *et al.*, 1938) using N_2 and were 200–250 m^2/g for "as prepared" clay and 150–220 m^2/g for calcined material.

A JEOL 4000 EX operated at 400 kV was used to perform high-resolution imaging. A VG HB501 dedicated scanning-transmission electron microscope (STEM) operated at 100 kV was used to obtain annular dark-field (ADF) images and energy-dispersive

[†] Present address: Gatan Inc., 6678 Owens Dr., Pleasanton, California 94588, USA.

[‡] Present address: Northboro R&D Center, Saint-Gobain Norton, Goddard Road, Northboro, Massachusetts 01532-1545, USA.

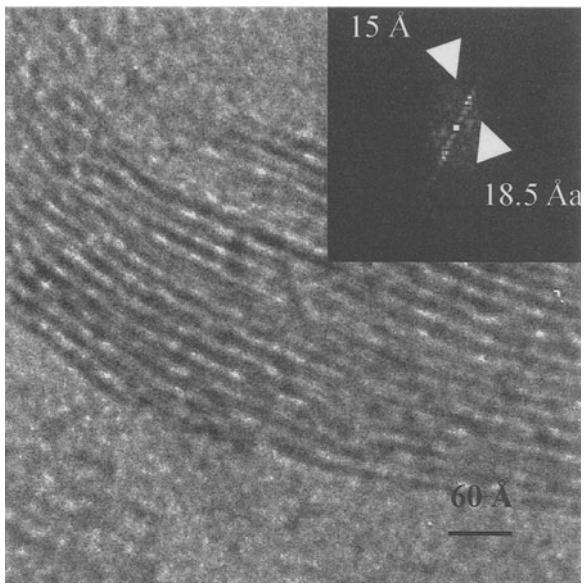

Figure 1. High-resolution image of pillared clay showing microstructural layering along the basal plane.

X-ray spectra (EDX) from the pillared montmorillonite. We used a LEO 912 microscope to perform energy-filtered analysis of the clay.

RESULTS AND DISCUSSION

Initial attempts were made to view pillared samples prepared for TEM by microtomy. Figure 1 shows a high-resolution image from a typical region of the pillared clay using low-dose conditions (Pan and Crozier, 1993) to avoid electron-beam damage to the clay structure. In this orientation, individual (001) layers of the clay can be seen clearly (the dark and light lines are lattices fringes). The insert, obtained by taking the Fourier transform of the image, shows the presence of spacings of 15 and 18.5 Å in this region of the clay. The 18.5-Å spacing is in good agreement with XRD measurements. The spacing of 15 Å is probably evidence for partial collapse of some of the layers in this region. Microtoming is useful to determine the degree of crystallinity and disordering in the clays. However, we were unable to unambiguously identify the zirconia pillars because the sample was too thick (microtomed sections are typically 300–600 Å thick).

The easiest way of imaging the pillars is to obtain small platelets only a few layers in thickness and to view these crystallites along the [001] or "basal plane projection". A successful approach for preparing such TEM samples is to grind the clay and to suspend in it water by dispersing with an ultrasonic probe. Then, a drop of the mixture is placed on a holey carbon film. Very small ultrathin platelets lying on the basal plane were then imaged.

Figure 2 shows bright-field images from the LEO microscope obtained from thin regions of a pillared and unpillared montmorillonite in the [001] projection. A small objective aperture (collection semi-angle = 4.3 mrad) was used for imaging to reduce phase contrast and to enhance sensitivity for regions of higher-mass density. (Underfocusing the objective lens was also found to enhance the contrast from dark features). The image from the pillared clay (Figure 2b) shows the presence of dark patches which are not present in the unpillared sample (Figure 2a). These patches are

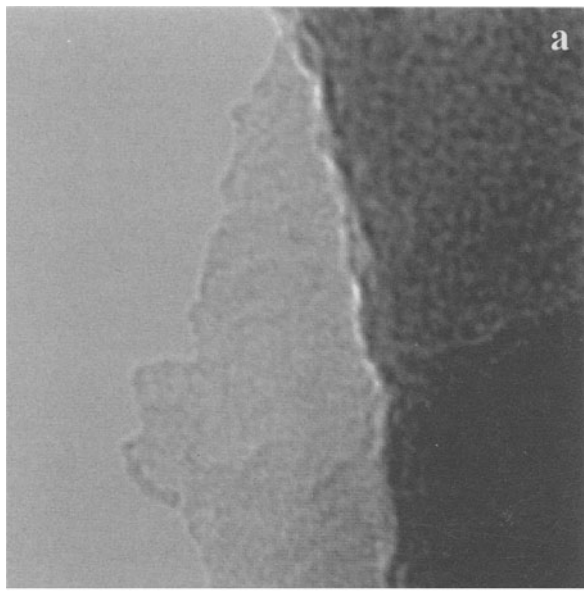

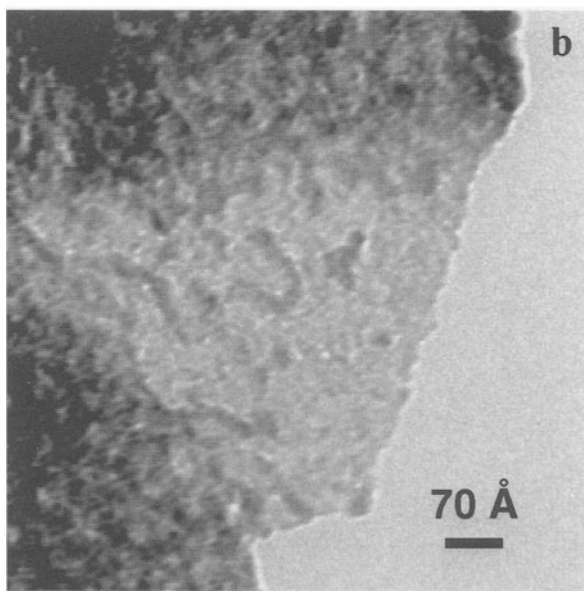

Figure 2. Bright-field images of platelet of (a) unpillared clay and (b) pillared montmorillonite. The images were recorded using a small objective aperture (4.3 mrad) to enhance the contrast (scale bar applies to both images).

https://doi.org/10.1346/CCMN.1999.0470601 Published online by Cambridge University Press

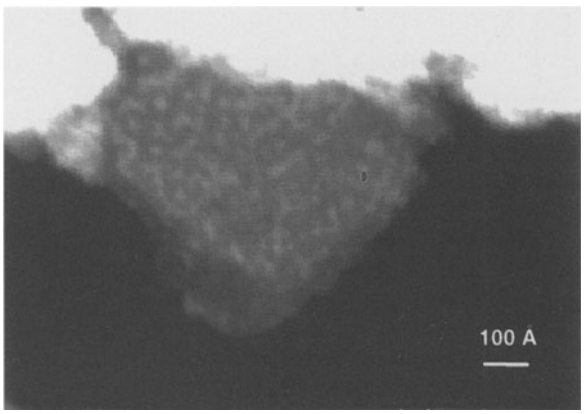

Figure 3. An ADF STEM image recorded from the pillared materials showing bright regions (which indicate higher atomic number).

between 10–50 Å in size and irregular in shape. Isolated patches are only visible in the thinnest regions of the sample, presumably because in thicker areas, overlap between the patches degrades visibility.

To confirm that the patches present in Figure 2b were indeed zirconia pillars, a number of analytical techniques were applied. An ADF STEM image from a similar region is shown in Figure 3. The ADF image is formed by collecting electrons scattered through large angles as the electron probe is rastered over the sample. For sufficiently high angles, the electron scattering has a strong dependence on the average atomic number of the sample (Treacy *et al.*, 1980; Treacy and Rice, 1989). In an ADF image, bright contrast corresponds to regions of high atomic number. The presence of light patches indicates higher atomic-number regions <50 Å in size with a morphology similar to the dark regions in Figure 2b. EDX was used to determine the local chemical composition of different parts of the clay. Spectra were taken from small light patches and regions between patches using a STEM probe of ~10 Å in diameter. Figure 4a and 4b shows spectra obtained from both the light patches and surrounding darker regions (Figure 3), respectively. Figure 4a clearly shows an enhancement of the L and K lines of Zr at 2.04 and 15.75 keV, respectively. This enhancement proves that the patches observed in Figures 1 and 2 are Zr-rich. Some Zr also shows in the spectra recorded between the patches. This Zr signal is probably a spurious effect caused by the extended tails on the electron probe that produce a non-local contribution to the X-ray spectrum. However, the important point is the factor of 2–3 increase in the Zr/Si ratio that is consistently obtained from the light regions.

Chemical analysis of the clay was also obtained by applying energy-filtered imaging to generate an elemental map from the electron energy-loss spectrum

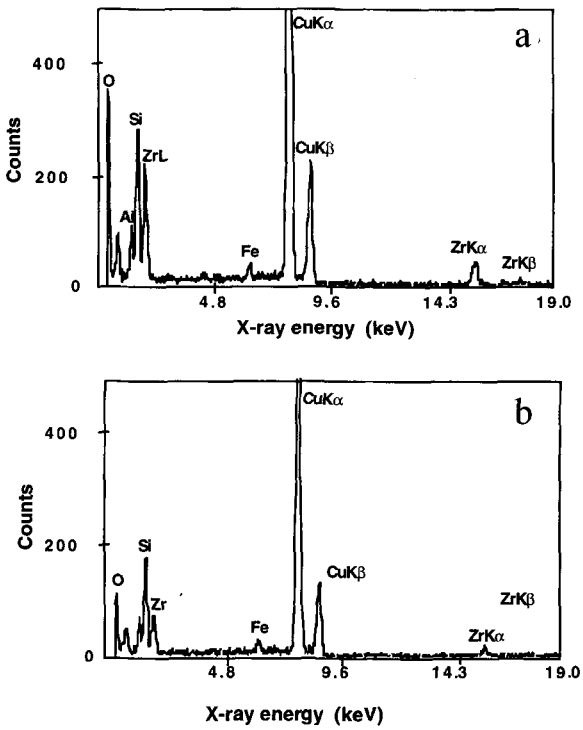

Figure 4. High-spatial resolution EDX spectra recorded from 20-Å regions from the platelet shown in Figure 2. Spectrum (a) is recorded from one of the light patches and shows an enhanced Zr signal and (b) is recorded from a darker region and shows a much weaker Zr signal.

(EELS). The energy-loss spectrum contains ionization edges characteristic of elements in the sample. The LEO 912 energy-filtering microscope is equipped with an in-column spectrometer and an energy-selecting slit, both of which can be used to select a particular energy loss for imaging. By appropriate choice of the energy-loss, electron images can be generated from spectroscopic information about an element. See Crozier (1995) for a detailed description of this technique.

The energy-filtering experiments were performed on the sample region shown in Figure 2b, and Figure 5 shows a typical energy-loss spectrum from the clay platelet. The spectrum shows a main low-loss peak at ~25 eV that corresponds to plasmon excitation and a second peak with an onset close to 40 eV that corresponds to the Zr N-edge. Figure 6a and 6b shows the energy-filtered images recorded from the clay using the Zr pre-edge region at 36 eV and the post-edge region at 43 eV energy loss, which corresponds to the maximum of the Zr peak. A slit width of ~5 eV was used.

Figure 6 shows structure similar to that of Figure 2, except the contrast is reversed because energy-filtered images are dark-field images. Evidence exists for etching the thin-clay layer because of the high electron doses needed to perform energy-filtered imaging. The

https://doi.org/10.1346/CCMN.1999.0470601 Published online by Cambridge University Press

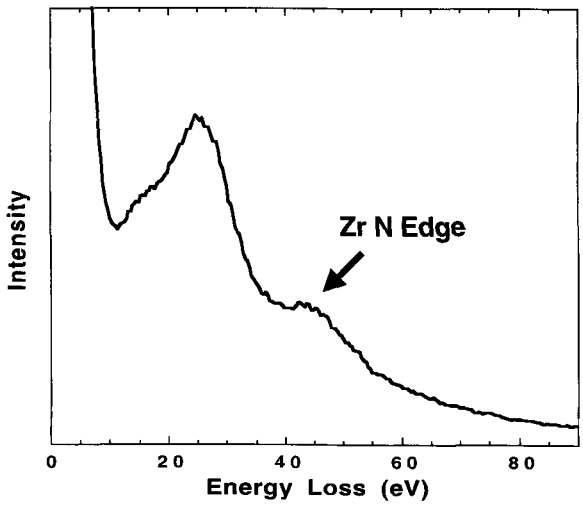

Figure 5. Electron energy-loss spectrum from pillared clay showing the Zr N_{23} edge used to form the Zr elemental map. To perform elemental mapping, images are recorded from the pre-edge and post-edge region.

image recorded with the Zr edge shows greater contrast at the pillar structures. However, to obtain a more accurate representation of Zr distribution, the background below the Zr edge must be removed to obtain an image that represents only the Zr distribution. Several ways to accomplish this are discussed in the literature. We used a simple method that involves scaling the post- and pre-edge images to give the same value in regions that have no pillars (Johnson, 1979). The scaled background image is then subtracted from the post-edge image. The error involved in this background correction should be small in the thinnest region of the crystal. The result of this operation is shown in Figure 6c. The image is more noisy but gives a better representation of the distribution of zirconia pillars in the clay. The elemental identification from energy-filtered mapping confirms the results obtained from X-ray mapping and ADF imaging.

CONCLUSION

The three analytical techniques demonstrate conclusively that zirconia pillars in montmorillonite can be directly imaged in very thin samples in the [001] orientation. The pillars can be imaged using three different signals: amplitude contrast in conventional bright-field TEM, ADF imaging in a dedicated STEM, and elemental mapping in an energy-filtering microscope. The energy-filtering technique is useful for confirming the composition of the pillars but requires a large electron dose which may result in damage to the clay. However, the damage does not appear to substantially alter the morphology of the pillars (compare the damaged region of Figure 6 with the same undamaged region of Figure 2). However, future studies on this material can use the more straightforward bright-field imaging approach to rapidly characterize the pillar structure in different zirconia-pillared systems.

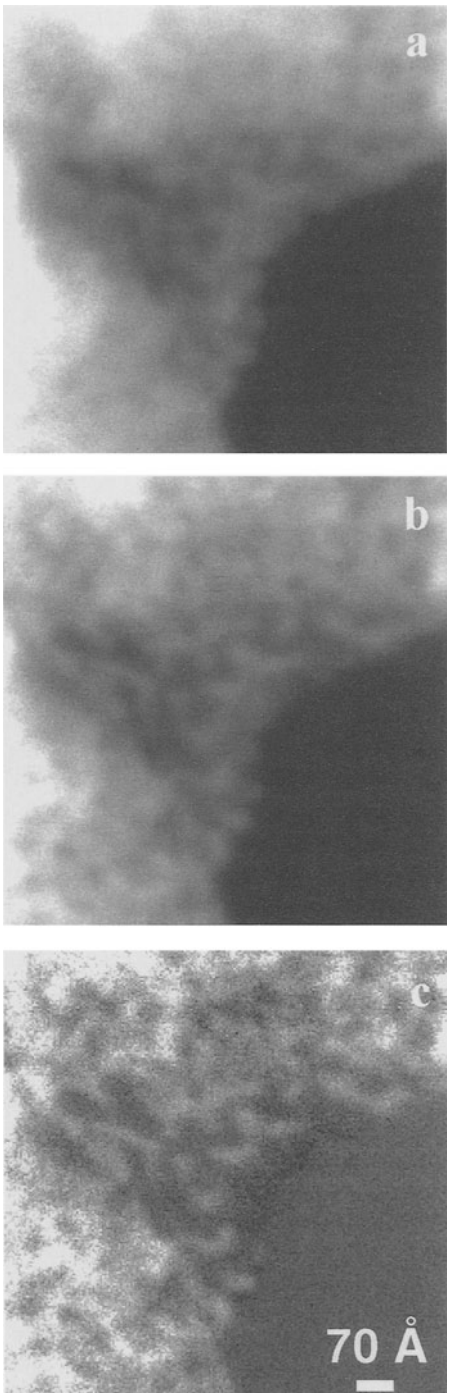

Figure 6. Energy-filtered images from (a) Zr pre-edge region at 36 eV and (b) the post-edge region at 43 eV. (c) Zr elemental map derived from (a) and (b) [scale bar applies to (a), (b), and (c)].

For the zirconia-pillared clay studied, the pillar structure appears to consist mainly of irregularly

https://doi.org/10.1346/CCMN.1999.0470601 Published online by Cambridge University Press

shaped regions <50 Å in size. Some curved elongated structures, 10–20 Å wide and <200 Å in length, can be observed. In principle, the same approach may be useful to image pillars composed of other elements. However, when pillars are composed of the same elements as the clay matrix, energy-filtered imaging and annular dark-field imaging may be less useful. On the other hand, bright-field amplitude contrast with a small objective aperture may be fruitful for extremely thin crystals in the correct orientation.

ACKNOWLEDGMENTS

Funding for this project was provided by UOP and the Industrial Associates Program of Arizona State University.

REFERENCES

Bartley, G.J. (1988) Zirconium pillared clays. *Catalysis Today,* **2,** 233–243.

Brunauer, S., Emmett, P.H., and Teller, E. (1938). Adsorption of gasses in multimolecular layers. *Journal of the American Chemical Society,* **60,** 309–320.

Crozier, P.A. (1995) Quantitative elemental mapping of materials by energy-filtered imaging. *Ultramicroscopy,* **58,** 157–174.

Crozier, P.A. and Pan, M. (1995) Quantitative nano-characterization of heterogeneous catalysts. In *Microscopy and Microanalysis Proceedings,* G.W. Bailey, M.H. Ellisman, R.A. Hennigar, and N.J. Zaluzec, eds., Jones and Begell Publishing, Boston, 398–399.

Datye, A.K. and Smith D.J. (1992) The study of heterogeneous catalysts by high resolution transmission electron microscopy. *Catalysis Reviews in Science and Engineering,* **34,** 129–178.

Johnson, D.E. (1979) *Energy Loss Spectrometry for Biological Research. Introduction to Analytical Electron Microscopy.* Plenum Press, New York.

Mitchell, I.V. (1990) *Pillared Layered Structures: Current Trends and Applications.* Elsevier Applied Science, New York, 256–257.

Pan, M. and Crozier, P.A. (1993) Low-dose high-resolution electron microscopy of zeolite materials with a slow scan CCD camera. *Ultramicroscopy,* **48,** 332–340.

Treacy, M.M.J. and Rice S.B. (1989) Catalyst particle sizes from Rutherford scattered intensities. *Journal of Microscopy,* **156,** 211–234.

Treacy, M.M.J., Howie, A., and Pennycook, S.J. (1980) Z contrast of supported catalysts particles on the STEM. *Institute of Physics Conference Series,* **52,** 261–264.

Vaughan, D.E.W., Lussier, R., and Magee, J. (1979) U.S. Patent 4,175,090.

Vaughan, D.E.W., Lussier, R., and Magee, J. (1980) U.S. Patent 4,248,739.

E-mail of corresponding author: Crozier@asu.edu

(Received 6 June 1997; accepted 25 October 1998; Ms. 97-052)